Cell Communication and Signaling

RESEARCH

Open Access

Atomoxetine suppresses radioresistance in glioblastoma via circATIC/miR-520d-5p/Notch2-Hey1 axis

Hyun Jeong Seok[1,2], Jae Yeon Choi[1], Dong Hyeon Lee[1], Incheol Shin[2] and In Hwa Bae[1*]

Abstract

Background Resistance acquired after radiotherapy is directly related to the failure of various cancer treatments, including GBM. Because the mechanism for overcoming radioresistance has not yet been clearly identified, the development of diagnostic and therapeutic markers to treat radioresistance is necessary. Since increased expression of stemness- and EMT-related markers are reported to be closely correlated with radioresistance, research is underway to develop new drugs targeting these factors.

Methods To develop an anticancer drug that overcomes radioresistance, a library of drugs already approved by the FDA was used. After treating radioresistant GBM cells with each drug, the expression of stemness- and EMT-related markers was confirmed by qRT-PCR, and as a result, Atomoxetine (ATX) was selected. It was confirmed that radioresistance-induced cell migratory, invasive, sphere formation abilities, and tumor growth using a xenograft mouse model were suppressed upon ATX treatment. Using a miRNA prediction tool, we discovered miR-520d-5p, which targets Notch2 and Hey1, key factors in radioresistance, and discovered circATIC targeting this miRNA, revealing its relationship with ATX. We demonstrated the expression regulation mechanism and signaling mechanism between circATIC, miR-520d-5p, Notch2, and Hey1 factors using a luciferase reporter assay. In addition, the results at the cellular level were clinically verified by confirming the correlation between radiation, miR-520d-5p, and circATIC using patient plasma by qRT-PCR.

Results ATX showed potential as a treatment for radioresistance by suppressing the malignant phenotype by regulating the circATIC/miR-520d-5p/Notch2-Hey1 signaling mechanism in vitro and in vivo using radioresistant GBM cells.

Conclusions This study revealed that ATX suppresses radioresistance through the circATIC/miR-520d-5p/Notch2-Hey1 signaling pathway. These results showed the potential of ATX as a new drug that can overcome radioresistance, a major challenge in cancer treatment, and the signaling factors identified in this mechanism suggest the possibility of use as potential targets for the diagnosis and treatment of radioresistance.

Keywords Glioblastoma, Radioresistance, Atomoxetine, Tumorigenicity, miR-520d-5p, circATIC, Notch2, Hey1

*Correspondence:
In Hwa Bae
ihbae@kirams.re.kr
[1] Division of Radiation Biomedical Research, Korea Institute of Radiological & Medical Sciences, Seoul, Republic of Korea
[2] Department of Life Science, Hanyang University, Seoul, Republic of Korea

Glioma is the most common primary malignant tumor in the central nervous system (CNS), and glioblastoma (GBM) remains one of the most aggressive and lethal cancers of the brain tumor. Standard treatment for GBM includes surgery, radiotherapy, and chemotherapy [1, 2]. Despite 30 years of intensive efforts to find effective chemotherapy for GBM, the 5-year survival rate for GBM patients is only 4–7% [2–5]. Repopulation by tumor cells

that survive radiotherapy limits the efficacy of subsequent radiotherapy and is a major cause of radiotherapy failure [6]. Additionally, according to Ali et al., radioresistance is caused by tumor microenvironment, hypoxia conditions, reprogramming of cellular energy or metabolic changes, glioma stem cells, tumor heterogeneity, microRNA, cell cycle, DNA repair, and other signaling pathways [7]. According to several papers, GBM recurrence is known to be caused by cancer stem cells with strong endogenous or treatment-induced radioresistance [6, 8, 9]. Therefore, approaches to treat tumors by targeting cancer stem cells have recently been attempted [10]. To overcome the malignant transformation of GBM, it is important to develop radioresistance mechanisms and identify specific therapeutic targets.

Drug repurposing (also known as drug repositioning) involves adapting an already approved drug to treat a new disease or advancing a previously studied but unapproved drug [10]. Since it is a drug on which much research has been conducted, it has the advantage of being cheaper than the cost of developing a new drug when applied to other diseases to change the drug's purpose [11]. For example, tamoxifen was developed as a contraceptive but failed because it did not suppress ovulation. However, it is currently a widely used drug for the treatment of breast cancer because it effectively inhibits estrogen and delays the growth of ER + breast cancer [12]. Doxorubicin, developed as an antibiotic from the Streptomyces peucetius bacterium, is used to treat soft tissues, bone sarcomas, breast cancer, ovarian cancer, bladder cancer, thyroid cancer, and blood cancers including lymphoblastic leukemia, acute myeloblastic leukemia, and Hodgkin lymphoma [13, 14]. Additionally, drugs approved for the treatment of breast cancer, such as cyclophosphamide, thiotepa, capecitabine, orouracil, gemcitabine, methotrexate, and palbociclib, are repurposed drugs [15]. Therefore, drug discovery through drug repurposing is actively used as an approach to treat many diseases, including cancer treatment [16–19].

Atomoxetine (ATX) is a non-stimulant and selective norepinephrine reuptake inhibitor used to treat attention-deficit/hyperactivity disorder (ADHD) [20]. In a previous study, ATX was studied to induce apoptosis, increase cytosolic and mitochondrial reactive oxygen species, changes in mitochondrial mass, membrane potential, and autophagy in neuron-like cells in a concentration-dependent manner [21]. However, the effect of ATX on cancer has not yet been reported. We discovered ATX by screening for drugs that most significantly reduced the expression of stemness maintenance and EMT-related markers in radioresistant cells. We found that ATX-induced miR-520d-5p suppresses tumorigenicity of radioresistant cells by reducing the expression of its targets, Notch2 and Hey1. In addition, the mechanism of action of ATX was studied by revealing that the expression of miR-520d-5p was downregulated by circATIC, which is a radiation resistance inducer and whose expression is decreased by ATX. Therefore, the mechanism by which ATX-mediated circATIC/miR-520d-5p/Notch2-Hey1 axis reduces radioresistance in GBM was newly revealed. These factors offer potential as new therapeutic targets for the treatment and diagnosis of radioresistance in GBM.

Materials and methods

Cell culture

Human glioma cell lines U373 and U87 were purchased from American Type Culture Collection (ATCC) and the Korea Cell Line Bank (KCLB), respectively. U373 and U87 cells were cultured in DMEM (Corning) containing 10% FBS (Corning) and 1% penicillin–streptomycin antibiotics (Welgene). Radioresistant cell lines U373R and U87R were established with 17 (U373R) and 12 (U87R) exposures of 5 Gy over 9 months, resulting in total exposures of 85 Gy (U373R) and 60 Gy (U87R), respectively. Cells were irradiated at a dose rate of 3.81 Gy/min using a 137Cs gamma-ray light source (Atomic Energy of Canada). Cells were cultured in a humidified incubator at 37 ℃ and 5% CO2. All cell lines were routinely tested for mycoplasma using the e-Myco™ Mycoplasma PCR Detection Kit (iNtRON) prior to use in experiments. 83NS cells were provided by Dr. Ichiro Nakano (University of Alabama at Birmingham, Birmingham, AL) [22]. 83NS, patient-derived GBM stem-like cells (GSCs), was maintained in DMEM-F-12 (Gibco) supplemented with B27 (Gibco), epidermal growth factor (EGF) (Sigma), human fibroblast growth factor (hFGF) (Biovision), and 5% penicillin–streptomycin (Corning) [23, 24].

Colony-formation assay

For colony formation analysis, cells were seeded at 1×10^3 in a 60 mm dish. After 24 h, parental and radioresistant cells were treated with radiation doses of 0, 3, 5, 10, 15, and 20 Gy. Colony formation assay was performed on cultures with regular medium changes for 14 days. Cells were stained with crystal violet and colony numbers were determined.

Cell proliferation assay

For proliferation assay, cells were seeded at 1×10^3 cells/well in a 96-well plate. After 24 h, both parental and radioresistant cells were treated with radiation doses of 0, 5, 10, 15, and 20 Gy, or with ATX at concentrations of 0, 10, 20, 30, 40, 50, 60, and 70 μM, or with TMZ at concentrations of 0, 250, 500, 750, and 1000 μM. After 48 h, cell proliferation was measured at 450 nm by adding

3-(4,5-dimethylthiazol-2-yl)-2,5-diphenyltetrazolium bromide (MTT; M2128, Sigma) reagent following washing with PBS. To determine time-dependent proliferation, U87R and U373R cells were treated with TMZ (750 μM, S1237, Selleck Chemicals) or ATX (25 μM, S3175, Selleck Chemicals), followed by the addition of MTT reagent at 0, 24, 48, and 72 h, and the absorbance was measured at 450 nm.

Drug library screening

We purchased a library of 774 FDA-approved drugs from Enzo Life Sciences (SCREEN-WELL FDA-approved drug library V2, BML-2843–0100, NY). Radioresistant U373 and U87 cells were seeded at 2×10^4 cells per well of a 96-well plate. Cells in each well were treated with 20 μM of test compound (Enzo #BML-2843–0100, SCREEN-WELL FDA-approved drug library V2) or control (DMSO, D8418, Sigma) for 48 h, and then harvested. The mRNA expression of stemness and EMT-related markers was confirmed using qRT-PCR.

RNA extraction and qRT-PCR analysis

Total RNA from U373 and U87 cells or mouse and human plasma was extracted using TRIzol reagent following the manufacturer's instructions. mRNA was synthesized using a cDNA Synthesis Kit, and miRNA was synthesized using a Mir-X miRNA First-Strand cDNA Synthesis Kit, respectively. qRT-PCR was performed using a LightCycler® 96 instrument (Roche) with Power SYBR Green PCR Master Mix (Invitrogen). mRNA and miRNA were quantified with GAPDH and U6 (Takara), respectively. The sequences of the primers are listed in Table 1.

Protein extraction and western blot analysis

Cells were lysed using RIPA buffer containing Xpert protease inhibitor cocktail solution and Xpert phosphatase inhibitor cocktail solution. Protein concentration was analyzed using the Bradford assay. The total protein extract was separated by SDS-PAGE and transferred to a PVDF membrane (Millipore). After blocking with 5% BSA for 1 h, the PVDF membrane was

Table 1 Primer sequences used in this study

Primers for qRT-PCR	**Sequences (5′-3′)**	
Notch2	Forward	ATGACTGCCCTAACCACAGG
	Reverse	TGCAGTCATCTCCACTCCAG
Sox2	Forward	ATGCACCGCTACGACGT GA
	Reverse	CTTTTGCACCCCTCCCATT
Vimentin	Forward	GCTTGGAAACATCCACATCG
	Reverse	GAGAGGAAGCCGAAAACACC
Zeb1	Forward	ATGACTGCCCTAACCACAGG
	Reverse	TGCAGTCATCTCCACTCCAG
Slug	Forward	ACAGCGAACTGGACACACAT
	Reverse	TCACTCGCCCCAAAGATGAG
Twist	Forward	GAAGATCATCCCCACGCTG
	Reverse	AGGAAGTCGATGTACCTGGC
Hey1	Forward	AGCAGGTAATGGAGCAAGGA
	Reverse	GCGCGTCAAAGTAACCTTTC
GAPDH	Forward	CATCTCTGCCCCCTCTGCTGA
	Reverse	GGATGACCTTGCCCACAGCCT
circ0058058(circATIC)	Forward	GGTGGTGTCCACGGAGAT
	Reverse	CCAAGAGCGGTCAGGTTT
miR-34a-5p	Forward	TGGCAGTGTCTTAGCTGGTTGT
miR-93-5p	Forward	CAAAGTGCTGTTCGTGCAGGTAG
miR-205-5p	Forward	TCCTTCATTCCACCGGAGTCTG
miR-519d-5p	Forward	CCTCCAAAGGGAAGCGCTTTCTGTT
miR-520d-5p	Forward	CTACAAAGGGAAGCCCTTTC
miR-765	Forward	TGGAGGAGAAGGAAGGTGATG
Primers for overexpression vector	**Sequences (5′-3′)**	
circ0058058(circATIC) overexpression	Forward	GCGAATTCCCTTATTTAGTGTCTCTGACAAAACCG
	Reverse	CGGCGGCCGCCTTCAAGGCTAACTGGCGTCTAG

incubated overnight at 4 ℃ with the primary antibody, which was diluted in BSA. Antibodies against Notch2 (#5732), Vimentin (#5741), Snail (#3879), Sox2 (#2748), Oct4 (#2750), and Zeb1 (#3396) were purchased from Cell Signaling Technology. Antibodies against Slug (sc-166476) and β-Actin (sc-47778) were obtained from Santa Cruz Biotechnology. Antibody against Twist (ab50887) was purchased from Abcam. Washed with TBS-T and treated with secondary antibody diluted in 5% skim milk. After washing with TBS-T, the membrane was treated with ECL solution and detected using an Amersham TM Imager 600 system (GE Healthcare).

Overexpression vector, siRNA, miRNA and transfection

To make the circATIC overexpression vector, we referred to the primer sequence in the paper by Zhang K et al. [25]. We purchased pcDNA3.1(+) CircRNA Mini Vector (Plasmid #60648) from addgene and created an overexpression vector. siNotch2 (sc-40135) and siHey1 (sc-37914) were purchased from Santa Cruz Biotechnology. Transfection was performed using the overexpression vector or RNA oligoribonucleotides using Lipofectamine 2000 reagent or G-fectin.

Wound healing migration assay

Transfected parental and radioresistant cells or ATX-treated cells were seeded in 6 well plate. After 24 h, monolayers were scratched with a yellow tip and changed the media. After 24 h, pictures were taken using a microscope (Miotic AE31 series) and the number of migrated cells was counted.

Transwell invasion assay

Invasion assays were performed by coating matrigel (#354234, BD) onto transwell chambers (Corning). 2.5×10^4 cells were placed in the upper transwell chamber, and conditioned medium containing 10% bovine serum albumin was added to the lower chamber. After 16 h, the upper chamber was fixed in methanol for 15 min and then stained with crystal violet. We took pictures under a microscope (Miotic AE31 series) and measured the number of cells.

Sphere formation assay

1×10^5 cells were seeded at 60 mm in Dulbecco's modified Eagle's medium-F12 (Corning, NY, USA) containing B27 (1:50) (Gibco) for 7–10 days. Spheres > 20 μM in diameter were counted using an inverted microscope (Miotic AE31 series).

Subcutaneous xenograft animal model

We xenografted parental U87 and radioresistant U87R cells subcutaneously into the right thigh of six-week-old female BALB/c nude mice (Orient Bio Inc), respectively. One week later, 20 mg/kg of ATX was injected intraperitoneally once a day, for a total of 5 days. After 2 weeks of cell injection, IR (10 Gy) was locally administered to the tumor site. The mouse model was irradiated at a dose rate of 2 Gy/min using an X-RAD 320 irradiator (PXi) equipment. After 12 days, mice were sacrificed and tumor size was examined. This animal experiment was reviewed and approved by the Institutional Animal Care and Use Committee (IACUC) of Korea Institute of Radiological & Medical Science (kirams2022-0131).

Dual luciferase reporter assay

The dual luciferase reporter assay used in the previous paper was performed as previously described [26]. To clone the reporter plasmid, pmirGLO vector (Promega) was purchased and the miR-520d-5p binding site of Notch2 and Hey1 3' UTR, as well as the miR-520d-5p binding site of circATIC were cloned. 293FT cells were seeded into 24-well culture plates according to the protocol, and then reporter plasmid (200 ng), pRL-CMV-Renilla plasmid (Promega) (2 ng), and miR-520d-5 p mimic were co-transfected with Lipofectamine 2000. Luciferase activity was measured using dual-luciferase reporter assay system (Promega) according to the manufacturer's instructions and normalized to Renilla luciferase activity.

Clinical specimen

Plasma from breast (KRB-2021-I002) and lung (KRB-2021-I002) cancer patients with and without radiation was provided by the Korea Institute of Radiology and Medical Sciences (KIRAMS) Radiation Biobank (KRB). All samples used in this experiment have completed the Institutional Review Board (IRB) of the Korea Institute of Radiology and Medical Sciences (KIRAMS) (KIRAMS 2021–04-002–001). Total RNA isolation and qRT-PCR were performed according to the indicated protocols.

Statistical analysis

All experiments were performed at least three times. All values are expressed as mean ± standard deviation. Statistical analysis was performed using GraphPad Prism 8 and analyzed using Student's t-test. A P value of $P<0.05$ was considered statistically significant. Detailed description of data, statistical methodology used, and sample size can be found at the end of the figure legend corresponding to each figure.

Results

ATX suppresses tumorigenicity in radioresistant GBM cells

To study how to overcome radioresistance in GBM, we established radioresistant GBM cells U373R and U87R

by repeatedly irradiating parental U373 and U87 cells with 5 Gy of radiation 17 and 12 times, respectively, over 9 months. In order to confirm the characteristics of the constructed radioresistant cells of U373 and U87, the parental and radioresistant cells were irradiated with various radiation doses (0, 5, 10, 15, and 20 Gy) and then their colony-forming abilities were compared using a clonogenic assay. As a result, the number of colonies in radioresistant cells increased in a dose-dependent manner compared to that in parental cells (Fig. S1A). Additionally, as a result of comparing the cell viability according to the radiation dose (0, 5, 10, 15, 20, 25, and 30 Gy), the survival rate was higher in the radioresistant cells compared to the parental cells (Fig. S1B). We identified the γ-H2AX protein to further confirm its radioresistance characteristics. γ-H2AX is a protein that repairs DNA damage and is associated with double-strand breaks (DSBs). Since γ-H2AX is a DSB-related protein and has the function of repairing DNA damage, analysis of the expression pattern of γ-H2AX is important among the key characteristics of resistant cell lines [27]. Expression of γ-H2AX peaked at 30 min in both parental and radioresistant cells. It then decreases dramatically at 3 h in resistant cells but remains stable in parental cells. These results suggest that radiation-induced DNA damage repair mechanisms are increased in radioresistant cells (Fig. S1C). These results showed that the U373 and U87 radioresistant cell lines were well established.

Drug repurposing (also known as drug repositioning) is the development of new uses for drugs already approved or in development and is an attractive strategy for discovering new treatments for diseases. To screen drugs that overcome the resistance mechanism of GBM, we treated GBM cells with a library of 774 FDA-approved drugs at the same concentration and screened eight drugs that inhibited cell proliferation. Then, we treated two radioresistant GBM cell lines, U373R and U87R, with the eight selected drugs, respectively, and screened for drugs that reduced the mRNA expression of stemness-related factors, Notch2 and Sox2, and EMT markers, Vimentin, Zeb1, Slug, and Twist (Fig. S2A, B). As a result, the drug ATX (D02, Atomoxetine) most dramatically reduced the mRNA expression of stemness and EMT markers. To confirm the cytotoxicity of ATX to radioresistant GBM cells, we treated ATX at various concentrations and confirmed cell viability by MTT assay (Fig. S2C). 20 μM of ATX was used in future experiments because it is a concentration that does not affect proliferation and cytotoxicity. Additionally, ATX is used as a drug (norepinephrine reuptake inhibitor) used to treat ADHD (Attention Deficit Hyperactivity Disorder) by inhibiting the reuptake of norepinephrine in brain nerve cells and enhancing the action of norepinephrine [20].

To determine the effect of temozolomide (TMZ), commonly used as a GBM treatment, on cell proliferation of radioresistant cells, parental and radioresistant U373 and U87 cells were treated with TMZ at concentrations of 250, 500, 750, 1000, and 1500 μM, respectively. Compared to two parental cells, TMZ resistance was observed in radioresistant cells, U373R and U87R. Therefore, we performed tumorigenic phenotype experiments by selecting 750 μM, a concentration of TMZ that does not show cytotoxicity in radioresistant cells (Fig. S3A). In order to discover a drug that effectively suppresses radioresistance, selected radioresistant GBM cells were treated with ATX (25 μM) and TMZ (750 μM), which are the IC50 concentrations of parantal cells (Fig. S3A), and their effects on radioresistant characteristics were compared. ATX inhibited the proliferation of radioresistant cells more effectively than TMZ (Fig. S3B). Additionally, to compare the effects of ATX and TMZ on tumor malignancy in radioresistant GBM cells, malignant phenotypes, migration, invasion, and sphere formation analysis were used. In U373R and U87R cells, motility (Fig. S3C), invasiveness (Fig. S3D), and sphere-forming ability (Fig. S3E) were reduced by ATX, but not TMZ. These results show that TMZ, a currently used GBM treatment, did not reduce tumorigenicity in GBM cells that acquired radioresistance, but ATX dramatically reduced these characteristics. Therefore, ATX suggests the possibility of being an alternative drug that can overcome the limitations of radioresistance treatment.To confirm the effect of ATX on radioresistant GBM cells, the expression of EMT and stemness-related markers, mobility, invasiveness, and stemness maintenance, which are representative phenotypic characteristics of malignant tumors, were confirmed. When radioresistant cells were treated with ATX, the expression of EMT markers Zeb1, Twist, Slug, and Vimentin and stemness-related markers Notch2 and Sox2 were reduced to levels similar to parental cells (Fig. 1A). Additionally, the migratory ability (Fig. 1B), invasiveness (Fig. 1C), and sphere formation ability (Fig. 1D) were reduced by ATX treatment in U373R and U87R cells. We confirmed that the expressions of Notch2 and Hey1 (Fig. 1E) and the stemness characteristic sphere-forming ability (Fig. 1F), which was increased by radiation in glioma patient-derived stem cells (GSCs) 83NS, were suppressed by ATX treatment. These results suggest the potential of ATX to overcome malignancy of resistant GBM cells.

According to Fig. 1A, Notch2 and Vimentin are the most significantly downregulated factors by ATX in resistant cells. Vimentin is a protein that acts as a cytoskeletal component such as microfilaments and microtubules and is known as the final product of the EMT process that plays a dynamic role in various basic

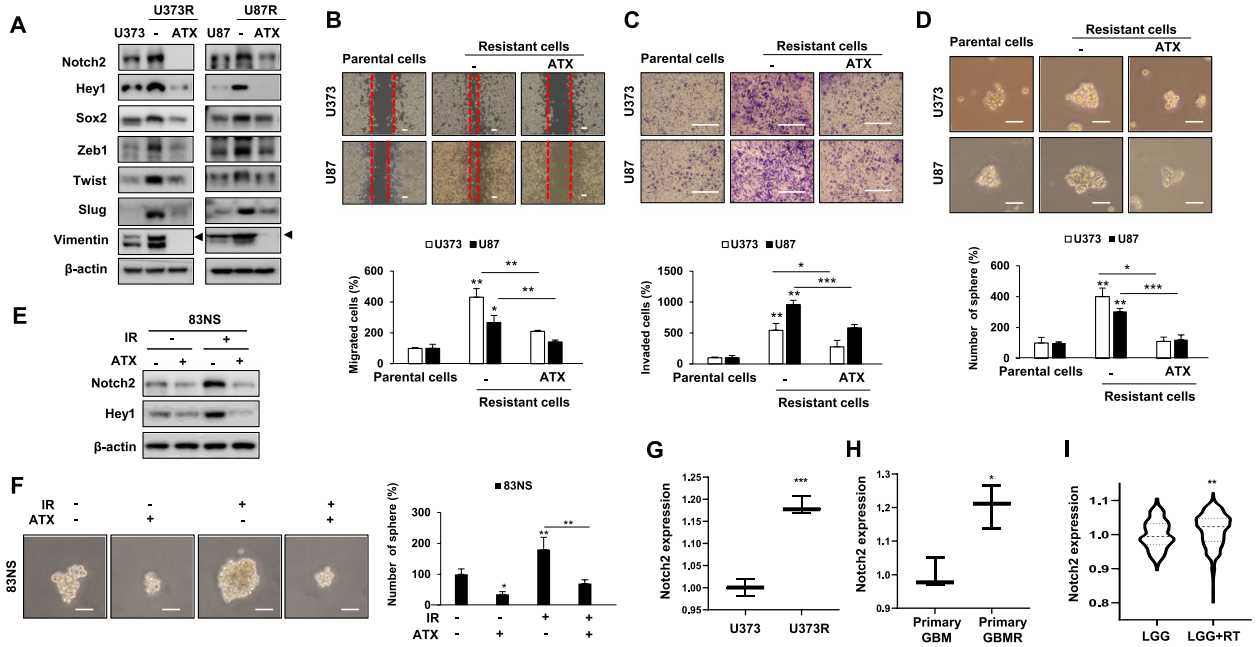

Fig. 1 ATX reduces the tumorigenicity of radioresistant GBM cells. **A**-**D** After treating radioresistant cells derived from U373 and U87 with ATX (20 μM), the tumorigenic phenotype was confirmed. **A** Expression of EMT and stemness-related markers was confirmed by western blot analysis. β-Actin was used as a loading control. The experiment was repeated with triplicates and representative western blotting images are shown. **B**-**D** Migratory ability (**B**), invasiveness (**C**), and stemness maintenance (**D**) were determined by wound healing (B, Scale bar, 100 μm), matrigel invasion (C, Scale bar, 100 μm), and sphere formation assays (D, Scale bar, 100 μm). **E**, **F** Expression of Notch2 and Hey1 in 83NS GBM patient-derived stem-like cells (GSCs) treated with IR (20 Gy) and ATX (20 μM) was determined using western blot analysis (**E**), and stemness capacity was determined using sphere formation assay (**F**) (F, Scale bar, 100 μm). β-Actin was used as a loading control. The experiment was repeated with triplicates and representative western blotting images are shown. **G**, **H** Using GEO public data (GSE199862), the expression of Notch2 was measured in U373 and U373R cells constructed by irradiating 2 Gy 5 times a week for a total of 60 Gy ($n=3$) (**G**), and in primary GBM and GBMR cells, constructed by irradiating 2 Gy 5 times a week for a total of 40 Gy ($n=3$) (**H**). **I** Through TCGA analysis using Xenabrowser (https:// xenabrowser.net), the expression of Notch2 was confirmed in patients of low-grade glioma ($n=174$) and those who received radiotherapy ($n=285$). The data are presented as the mean ± SD for triplicate experiments. *$P<0.05$, **$P<0.01$, and ***$P<0.001$. Student`s t-test

cellular processes such as structural support, adhesion, migration, and signaling [28–30]. On the other hand, Notch2 was selected as a key factor to analyze the signaling process between factors involved in the tumor suppression mechanism by ATX [31, 32]. To confirm whether Notch2 and Hey1 are involved in the tumorigenic ability of radioresistant cells, Notch2 and Hey1 were used as siRNA. The knockdown of Notch2 and Hey1 expression resulted in reduced radioresistant cells-induced the expression of factors involved in tumorigenicity, cell migration, invasion, and sphere formation ability (Fig. S4A-E). We further verified the relationship between radioresistance and expression of Notch2 through public data analysis using GEO dataset. In U373 (Fig. 1G) or primary GBM cells (Fig. 1H), Notch2 expression was found to be higher in radioresistant cells than in parental cells. Additionally, the relationship between brain tumor and Notch2 expression was confirmed through TCGA data analysis using xenabrowser. We found that Notch2 expression was increased in patients who received radiotherapy (RT) compared to those with low-grade glioma (LGG) (Fig. 1I). These results suggested that Notch2 and Hey1 are involved in the malignancy mechanism of resistant cells.

ATX increases the sensitivity of radiotherapy in vivo

To confirm the efficacy of ATX in vivo, parental and radioresistant U87 cells were injected subcutaneously into mice, respectively, followed by intraperitoneal administration of ATX (Fig. 2A). Tumor size and weight were compared after radiation treatment in mice injected with parental and resistant cells, respectively. Compared to mice injected with parental cells, mice injected with resistant cells showed greater resistance to radiation and did not reduce tumor size or weight. However, when ATX administration and radiation treatment were combined in mice injected with resistant cells, a significant reduction in tumor size and weight was observed (Fig. 2B, C). Additionally, the expression of Notch2 and Hey1 in tumor tissue and plasma of mice was confirmed. It was confirmed that the expression of Notch2 and Hey1, which was increased by radiation treatment, decreased in

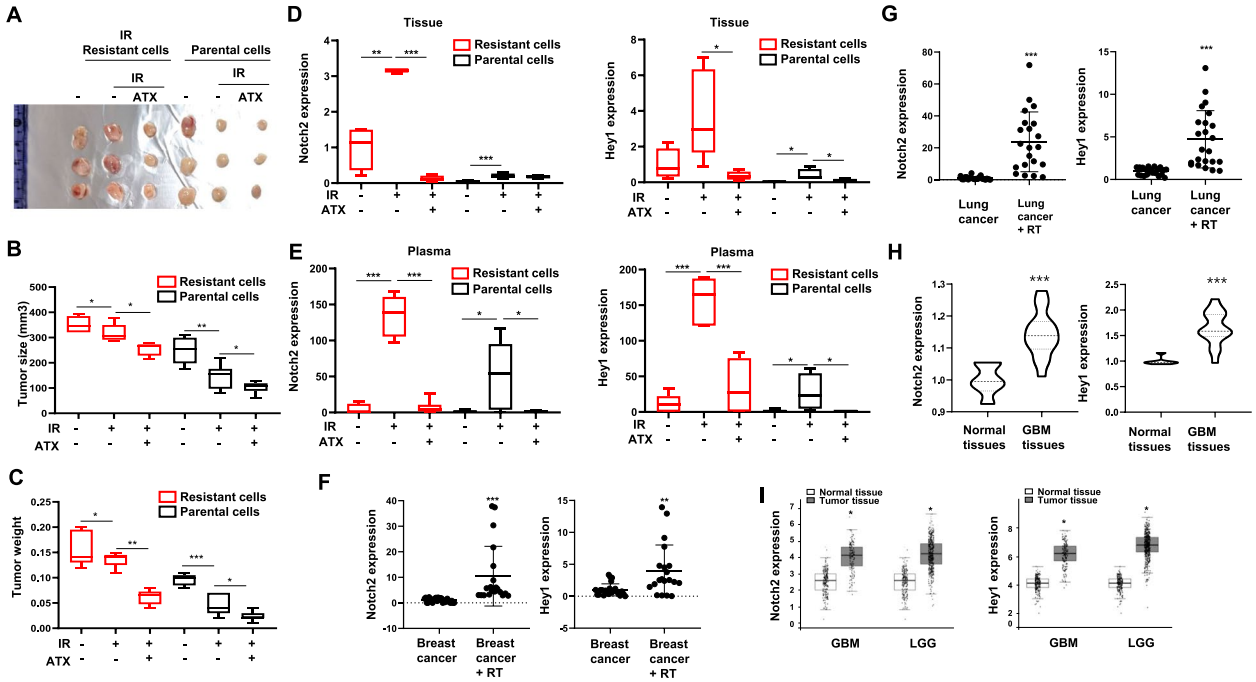

Fig. 2 ATX suppresses radioresistant GBM cells-induced tumor growth by inhibiting Notch2-Hey1 signaling. **A**-**C** Parental and radioresistant U87 cells (1×10^7 cells/mouse) were injected subcutaneously into the right thigh of mice. One week later, ATX (20 mg/kg) was injected intraperitoneally into the mouse once a day for a total of 5 times. Two weeks after cell injection, IR (10 Gy) was irradiated, and 12 days later, mice were sacrificed and tumor sizes (**A**, **B**) and body weight (**C**) were measured. (resistant cells, $n = 5$; resistant cells + IR, $n = 5$; resistant cells + IR + ATX, $n = 6$; parental cells, $n = 5$; parental cells + IR, $n = 7$; parental cells + IR + ATX, $n = 7$) **D**, **E** The expression of Notch2 and Hey1 in subcutaneous tumor tissues (**D**) and plasma (**E**) of ATX-treated radioresistant mice model was confirmed by qRT-PCR. qRT-PCR values were normalized by GAPDH. (Notch2 and Hey1 expressions in tissues and plasma of mice: resistant cells, $n = 5$; resistant cells + IR, $n = 5$; resistant cells + IR + ATX, $n = 6$; parental cells, $n = 5$; parental cells + IR, $n = 7$; parental cells + IR + ATX, $n = 7$) **F**, **G** The mRNA expression of Notch2 and Hey1 in the plasma of breast cancer (**F**) and lung cancer (**G**) patients with or without radiotherapy was confirmed using qRT-PCR analysis. (Notch2 expression: Breast cancer, $n = 27$; Breast cancer + radiotherapy (RT), $n = 20$; Lung cancer, $n = 20$; Lung cancer + RT, $n = 21$) (Hey1 expression: Breast cancer, $n = 24$; Breast cancer + RT, $n = 23$; Lung cancer, $n = 21$; Lung cancer + RT, $n = 23$) The values were normalized by GAPDH. **H**, **I** The expression of Notch2 and Hey1 was confirmed in GBM tissues and adjacent normal tissues through the GEO database (GPL17692) (Normal tissues, $n = 6$; GMB tissues, $n = 16$) (**H**) and GEPIA (Gene Expression Profiling Interactive Analysis) database (Normal tissues, $n = 207$; GBM tumor tissues, $n = 163$; LGG tumor tissues, $n = 518$) (**I**). I The data are presented as the mean ± SD for triplicate experiments. *$P < 0.05$, **$P < 0.01$, and ***$P < 0.001$. Student`s t-test

the ATX and irradiation combination group (Fig. 2D, E). These results suggest the possibility of ATX as a drug to overcome radioresistance in vivo.

The standard treatment for GBM is surgical resection followed by concurrent administration of the anticancer drug temozolomide (TMZ) and chemoradiotherapy [33]. Because of this treatment sequence, it is very difficult to obtain a number of irradiated GBM patient tissues. Therefore, we used plasma from breast and lung cancer patients with and without irradiation to determine the effect of irradiation on Notch2 and Hey1 expression. The results showed that the expression of Notch2 and Hey1 was higher in breast and lung cancer patients with radiotherapy compared to those without radiotherapy (Fig. 2F, G). These results indirectly support the results at the cellular level and in animal models.

In addition, to confirm the clinical significance of Notch2 and Hey1 in GBM, we utilized publicly available data of GBM patients (GEO database, GPL17692 and GEPIA (Gene Expression Profiling Interactive Analysis)) to determine the expression of Notch2 and Hey1 in GBM tissues and adjacent normal tissues. The expression of Notch2 and Hey1 was found to be higher in GBM tissues compared to adjacent normal tissues (Fig. 2H, I). Using the Chinese Glioma Genome Atlas (CGGA) database, we confirmed that the expression of Notch2 and Hey1 was positively correlated in recurrent gliomas (Fig. S5A). Additionally, KM plot analysis showed that high expression of Notch2 and Hey1 was associated with poor prognosis in patients with various cancers, including glioma, gastric adenocarcinoma (Fig. S5B, C). These results suggest that Notch2 and Hey1 expression is associated with poor prognosis of patients.

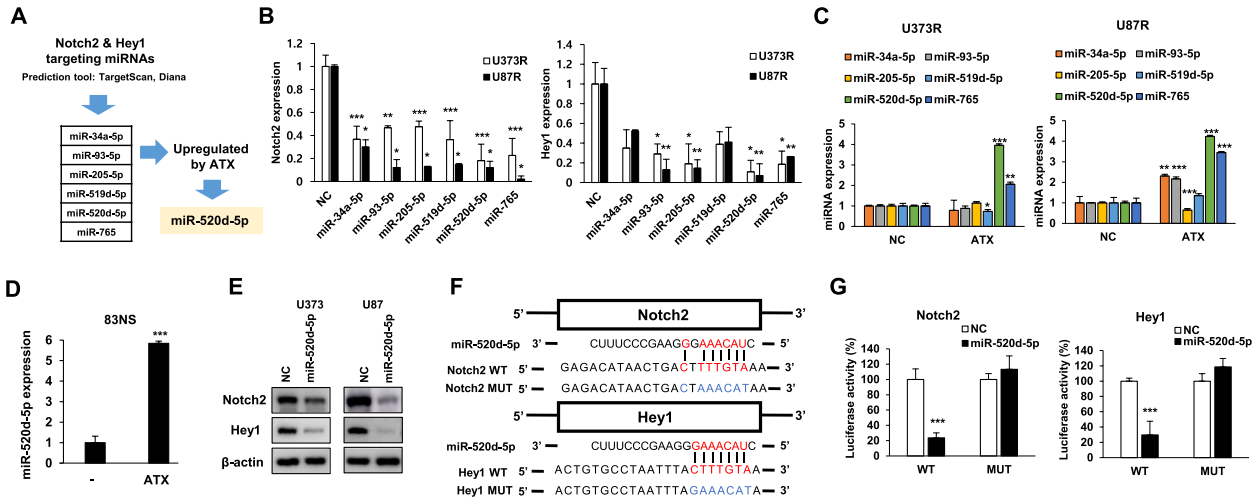

Fig. 3 Validation of miR-520d-5p, which directly targets Notch2 and Hey1 and is upregulated by ATX. **A** Using TargetScan and Diana, which are miRNA target prediction tools, we selected miR-520d-5p that were reduced by ATX among candidate miRNAs targeting Notch2 and Hey1. The Venn diagram briefly shows the selection of miR-520d-5p. **B** After transfecting six candidate miRNAs mimics (miR-34a-5p, miR-93-5p, miR-205-5p, miR-519d-5p, miR-520d-5p, and miR-765) that directly target Notch2 and Hey1 into U373R and U87R cells, the mRNA expression of Notch2 and Hey1 was compared by qRT-PCR analysis. **C** U373R and U87R cells were treated with ATX (20 μM), and the expression of candidate miRNAs was confirmed by qRT-PCR. **D** 83NS GBM patient-derived stem-like cells (GSCs) were treated with ATX and the expression of miR-520d-5p was confirmed by qRT-PCR. The qRT-PCR values were normalized by U6. **E** After overexpression of selected miR-520d-5p mimics in U373 and U87 cells, the protein levels of target factors Notch2 and Hey1 were confirmed by western blot analysis. β-Actin was used as a loading control in western blotting assay. The experiment was repeated with triplicates and representative western blotting images are shown. **F** The binding site for miR-520d-5p was indicated in the 3'UTR of Notch2 and Hey1. The pmirGLO luciferase vector was synthesized by creating wild-type (WT) and mutant (Mut) constructs of the binding site. **G** Luciferase activity was determined in 293FT cells transfected with firefly luciferase constructs. Firefly luciferase activity was normalized to *Renilla* luciferase activity for each sample. The data are presented as the mean ± SD for triplicate experiments. *$P < 0.05$, **$P < 0.01$, and ***$P < 0.001$. Student`s t-test

miR-520d-5p, which is upregulated by ATX, directly targets Notch2 and Hey1

To investigate the mechanism of reduced Notch2 and Hey1 expression by ATX, we screened for miRNAs that target Notch2 and Hey1 and are upregulated by ATX (Fig. 3A). After overexpression of six candidate miRNA mimics in U373R and U87R cells, we selected miR-520d-5p that most dramatically suppressed the expression of Notch2 and Hey1 (Fig. 3B) and was the most upregulated by ATX (Fig. 3C). In addition to the cellular level, using patient-derived GSCs, it was confirmed that the expression of candidate miR-520d-5p was increased upon ATX treatment (Fig. 3D). By overexpressing the selected miR-520d-5p mimic, a decrease in the protein levels of Notch2 and Hey1 was confirmed (Fig. 3E). A luciferase assay was performed to confirm whether the expression of miR-520d-5p was inhibited by directly binding to Notch2 and Hey1, two target factors. We identified the binding site of miR-520d-5p in the 3' UTR of Notch2 and Hey1 and designed reporter constructs containing wild type (WT) and mutant type (MUT) (Fig. 3F). Transduction of miR-520d-5p inhibited the respective activities of Notch2 and Hey1 in combination with WT, but had no effect on MUTs (Fig. 3G). These results demonstrate that miR-520d-5p directly binds to Notch2 and Hey1 and inhibits their expression.

miR-520d-5p reduces tumorigenicity of GBM by downregulating Notch2 and Hey1

To verify the relationship between the anti-tumor mechanism of miR-520d-5p and its targets, Notch2 and Hey1, U373R and U87R cells were transformed with siNotch2 or siHey1 in the presence or absence of the inhibitor of miR-520d-5p (anti-miR-520d-5p) (Fig. 4). As a result, stemness and expression of EMT markers (Fig. 4A, B) and the cell migration (Fig. 4C), invasive (Fig. 4D) and sphere formation (Fig. 4E) abilities increased by the miR-520d-5p inhibitor were restored by siNotch2 and siHey1. Our results showed that miR-520d-5p induced antitumor effects by suppressing the expression of Notch2 and Hey1 in radioresistant cells.

ATX reduces tumorigenicity of radioresistant GBM cells by upregulating miR-520d-5p

To determine whether ATX suppresses tumorigenicity by upregulating the expression of miR-520d-5p in radioresistant GBM cells, combination treatment with ATX or a miR-520d-5p inhibitor (anti-miR-520d-5p)

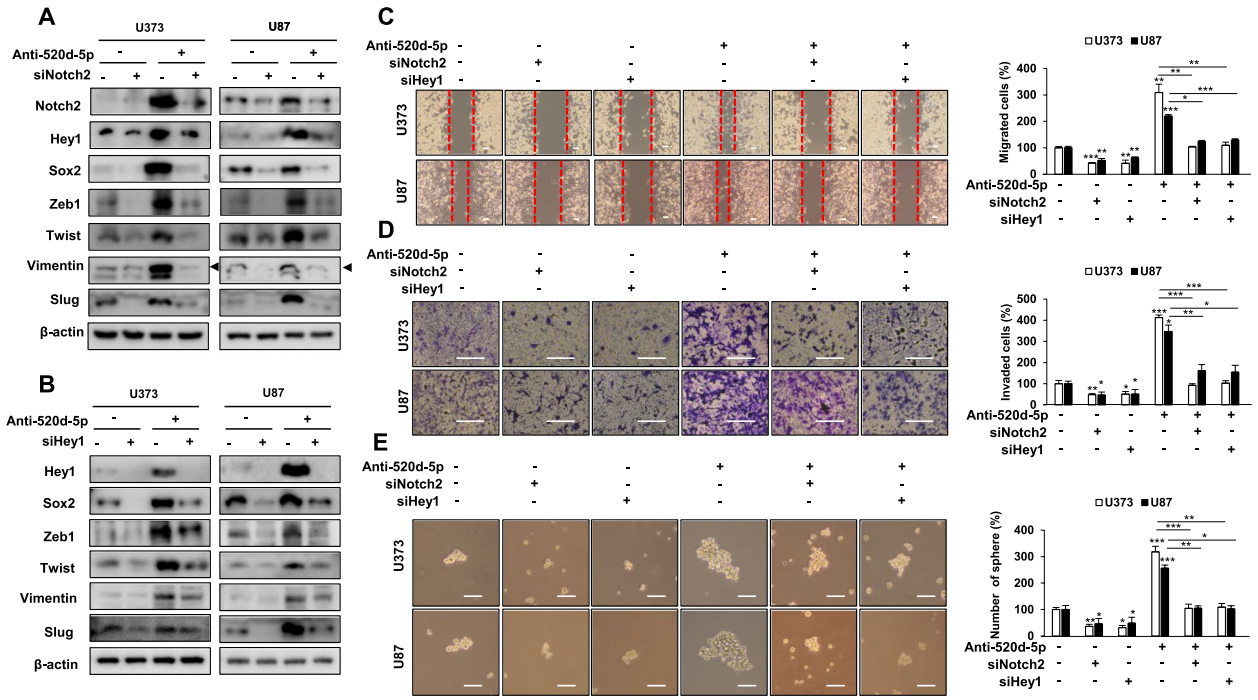

Fig. 4 miR-520d-5p suppresses the malignant phenotype of GBM by reducing the expression of Notch2 and Hey1. **A**-**E** U373 and U87 cells were transfected with the miR-520d-5p inhibitor and/or siNotch2 or siHey1, and the malignant phenotype was confirmed. **A**, **B** The expression of EMT and stemness-related markers was confirmed using western blot assay. β-Actin was used as a loading control in western blot assay. The experiment was repeated with triplicates and representative western blotting images are shown. **C**-**E** The migratory (**C**), invasive (**D**), and sphere formation abilities (**E**) were detected by wound healing (C, Scale bar, 100 μm), matrigel invasion (D, Scale bar, 100 μm), and sphere formation assays (E, Scale bar, 100 μm), respectively. The data are presented as the mean ± SD for triplicate experiments. *$P < 0.05$, **$P < 0.01$, and ***$P < 0.001$. Student`s t-test

was performed. ATX-suppressed the expression of stemness and EMT markers (Fig. 5A) and cell migratory (Fig. 5B), invasive (Fig. 5C), and sphere formation (Fig. 5D) abilities were restored by the inhibitor of miR-520d-5p (Fig. 5A-D). In addition, the expression of Notch2 and Hey1 (Fig. 5E) and sphere-forming ability (Fig. 5F) increased by miR-520d-5p inhibitor in GSC cells 83NS were suppressed by ATX treatment. These results suggest that ATX reduces the malignant properties of radioresistant GBM cells by increasing the expression of miR-520d-5p.

To confirm the expression of miR-520-5p in an animal model to overcome resistance by ATX, the expression of miR-520d-5p was confirmed in tumor tissues (Fig. 5G) and plasma (Fig. 5H) of xenograft mice injected subcutaneously with U373 or U373R cells. As a result, the expression of miR-520d-5p decreased in the radiation-treated group, but increased in the radiation and ATX combination treatment group. Additionally, the increase rate in the radiation and ATX combination treatment group was higher in the tissues and plasma of mice injected with radioresistant cells than with parental cells. Based on these results, it was confirmed that the inhibition of malignant characteristics by ATX in radioresistant cells was positively correlated with the high expression of miR-520d-5p.

To confirm the relationship between radiation and miR-520d-5p, we confirmed the expression of miR-520d-5p in the plasma of breast and lung cancer patients with or without radiotherapy. The expression of miR-520d-5p was low in breast (Fig. 5I) and lung cancer (Fig. 5J) patients with radiotherapy. To confirm the clinical correlation between GBM and miR-520d-5p, we confirmed the expression of miR-520-5p in surrounding normal and GBM tissues by GEO database analysis. Compared with surrounding normal tissues, the expression of miR-520d-5p was lower in GBM tissues (Fig. 5K). Survival curves of patients with various cancers, including glioma and gastric adenocarcinoma, showed that high expression of miR-520d-5p was associated with good prognosis of patients using KM plot analysis (Fig. 5L and S6). These clinical results show a positive correlation between patient survival and miR-520d-5p expression.

circATIC increases tumorigenicty by suppressing the expression of its target, miR-520d-5p

According to Chen D. et al. [34], 20 candidate circRNAs with high expression in radioresistant cells were selected.

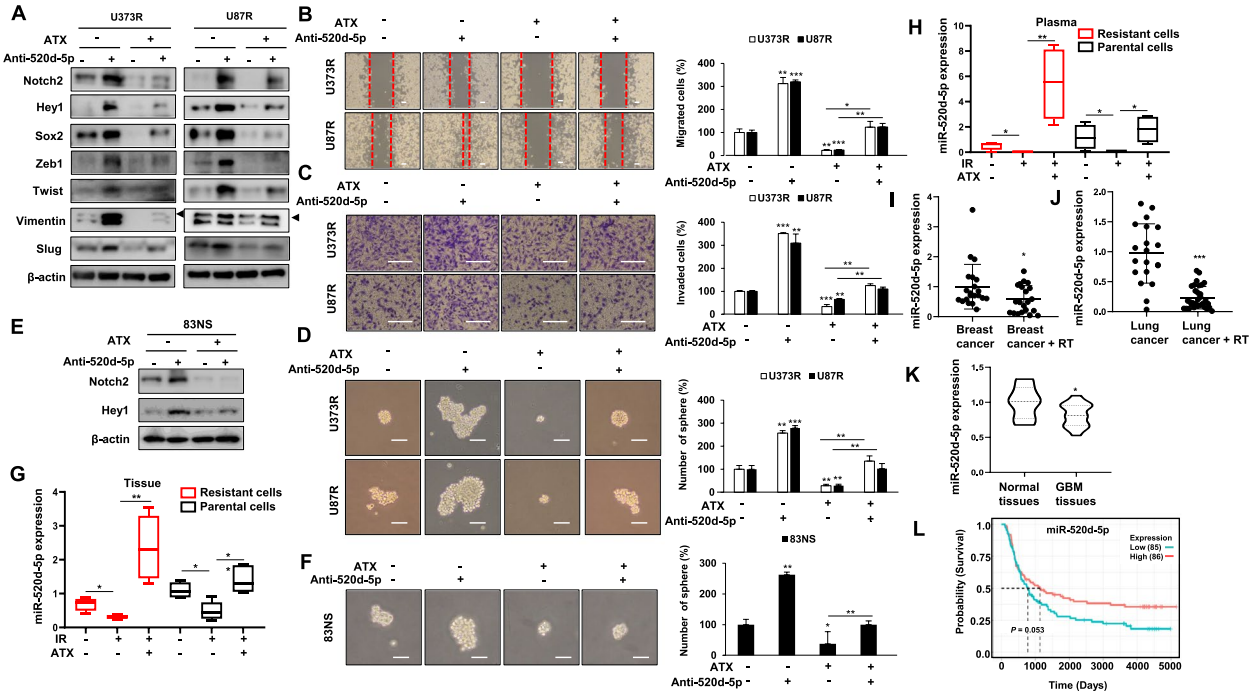

Fig. 5 ATX inhibits tumorigenicity of GBM by inducing the expression of miR-520d-5p. **A**-**D** After combined treatment of U373R and U87R cells with ATX (20 μM) or miR-520d-5p inhibitor, the expression of EMT and stemness-related markers **A** and the migratory (**B**), invasive (**C**), and sphere formation abilities (**D**) were detected by western blot, wound healing (B, Scale bar, 100 μm), matrigel invasion (C, Scale bar, 100 μm), and sphere formation assays (D, Scale bar, 100 μm), respectively. **E**, **F** After combining miR-520d-5p inhibitor and ATX in 83NS, glioma patient-derived stem cells (GSCs), Notch1 and Hey1 protein expression (**E**) and stemness maintenance (**F**) were determined by western blot and sphere formation assays, respectively. (F, Scale bar, 100 μm). The experiment was repeated with triplicates and representative western blotting images are shown. **G**, **H** The expression of miR-520d-5p in tumor tissues (**G**) and plasma (**H**) obtained after ATX treatment in subcutaneous xenograft mice injected with U87 or U87 was confirmed by qRT-PCR analysis. (miR-520d-5p expression in tumor tissues and plasma of indicated groups: resistant cells, $n=5$; resistant cells + IR, $n=5$; resistant cells + IR + ATX, $n=6$; parental cells, $n=5$; parental cells + IR, $n=7$; parental cells + IR + ATX, $n=7$) The qRT-PCR results were normalized by U6. **I**, **J** The expression patterns of miR-520d-5p were compared in breast cancer patients (**I**) and lung cancer patients (**J**) with or without radiotherapy (RT). (Breast cancer patients, $n=21$; Breast cancer patients + RT, $n=21$; Lung cancer patients, $n=20$; Lung cancer patients + RT, $n=21$). The values were normalized by U6. **K** Expression of miR-520d-5p was confirmed in a GEO database (GSE90604). **L** Using the Chinese Glioma Genome Atlas (CGGA), patient survival rates according to the expression pattern of miR-520d-5p were identified. The data are presented as the mean ± SD for triplicate experiments. *$P<0.05$, **$P<0.01$, and ***$P<0.001$. Student`s t-test

We used the prediction program tool to identify the circRNA targeting miR-520d-5p among these 20 candidate circRNAs (Fig. 6A). The genomic location and splicing pattern of circATIC, consisting of exons 2–6 of ATIC, is shown in a schematic diagram (Fig. 6B). To verify the selected circATIC, expression was compared in parental and radioresistant cells, and it was increased in radioresistant cells (Fig. 6C). In addition, it was confirmed that when circATIC was overexpressed (Fig. 6D), the expression of the target, miR-520d-5p, was decreased (Fig. 6E). We performed a luciferase assay to confirm whether circATIC directly binds to miR-520d-5p and acts as a sponge for miR-520d-5p by direct binding. Luciferase activity was reduced by miR-520d-5p when co-transfected with the WT construct, but there was no change in that of MUT (Fig. 6F). As a result of confirming the effect of the interaction between circATIC and miR-520d-5p on tumorigenicity, circATIC-increased the expression of stemness and EMT-related markers (Fig. 6G), cell mobility (Fig. 6H), invasiveness (Fig. 6I), and sphere forming ability (Fig. 6J) was reduced when treated with miR-520d-5p. These results suggest that circATIC, which is highly expressed in radioresistant cells, participates in the mechanism that increases tumor malignancy by directly reducing the expression of miR-520d-5p.

As a result of confirming the expression relationship between ATX and circATIC, the expression of circATIC was reduced when radioresistant U373R and U87R cells were treated with ATX (Fig. 7A). To analyze the role of circATIC in the mechanism of suppressing tumorigenicity by ATX, the tumorigenic phenotype was confirmed by combining circATIC overexpression with or without ATX treatment. Expression of stemness and EMT markers (Fig. 7B), migration (Fig. 7C), invasion (Fig. 7D) and sphere formation ability (Fig. 7E), which were reduced by ATX in U373R and U87R, were

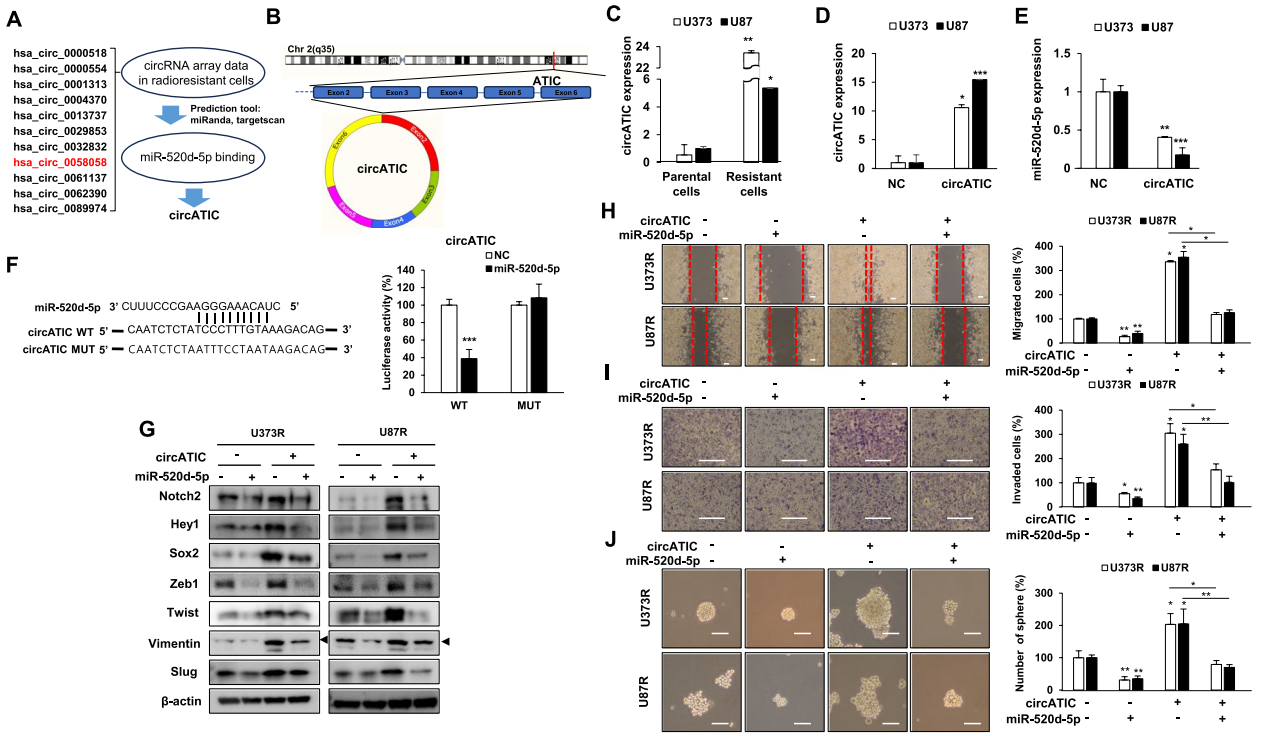

Fig. 6 circATIC is involved in the malignancy of GBM by suppressing the expression of miR-520d-5p. **A** hsa_circ_0058058 (circATIC), which is predicted to bind to miR-520d-5p and has increased its expression in radioresistant cells, was selected. **B** A schematic diagram of the genomic location and splicing pattern of circATIC is shown. **C** The expression level of circATIC in parental and radioresistant cells was confirmed by qRT-PCR. **D**, **E** After overexpressing circATIC in U373 and U87 cells, the expression of circATIC (**D**) and miR-520d-5p (**E**) was confirmed by qRT-PCR. The qRT-PCR results were normalized by U6 and GAPDH. **F** To confirm the direct binding of circATIC to miR-520d-5p, luciferase assay was performed. The binding sites of circATIC and miR-520d-5p were cloned into wild type (WT) and mutant type (MUT). Luciferase activity was measured after co-transfection of WT and MUT constructs with miR-520d-5p into 293FT cells. Firefly luciferase activity was normalized to the *Renilla* luciferase activity of each sample. **G**-**J** U373R and U87R cells were transfected with miR-520d-5p in the presence or absence of circATIC and the tumorigenic phenotype was confirmed. **G** Expression of stemness and EMT-related markers was confirmed by western blot analysis. β-Actin was used as a loading control. The experiment was repeated with triplicates and representative western blotting images are shown. **H**-**J** Cell mobility (**H**), invasiveness (**I**), and sphere formation ability (**J**) were measured using wound healing (H, scale bar, 100 μm), matrigel invasion (I, scale bar, 100 μm), and sphere formation assays (J, scale bar, 100 μm), respectively. The data are presented as the mean ± SD for triplicate experiments. *$P < 0.05$, **$P < 0.01$, and ***$P < 0.001$. Student`s t-test

restored by overexpressing circATIC. These results support the hypothesis that circATIC expression is reduced by ATX, thereby increasing the expression of its target, miR-520d-5p, thereby suppressing radiation malignancy.

In addition, the expression of circATIC in the tissues and plasma of ATX-injected xenograft animals was higher in the group injected with resistant cells than in the parental cells, and the expression was decreased by ATX (Fig. 8A-B). For radiological and clinical analysis, we confirmed the expression of circATIC in breast cancer (Fig. 8C) and lung cancer (Fig. 8D) patients. As a result, the expression of circATIC was increased in cancer patients who received radiotherapy. In a public data analysis using nasopharyngeal cancer (NPC) patient samples, the expression of circATIC was higher in tumor samples compared to normal tissues. Additionally, circATIC was more highly expressed in the tissues of relapsed patients compared to non-relapsed patients (Fig. 8E). Taken together, the expression of radioresistance-induced circATIC was reduced by ATX administration, which may be involved in improving the prognosis of cancer patients. We identified the circATIC/miR-520d-5p/Notch2-Hey1 axis as a radioresistance-induced tumor malignancy mechanism and suggested the potential of ATX as a therapeutic agent to suppress radioresistance (Fig. 8F).

Discussion

The development of new drugs involves the following very complex steps: 1) Study of disease mechanism and target, 2) Exploration and discovery of treatment strategy, 3) Study of mechanism of action and toxicity of candidate drug, 4) Clinical evaluation of drug in humans, 5) Drug approval decision and post-marketing monitoring

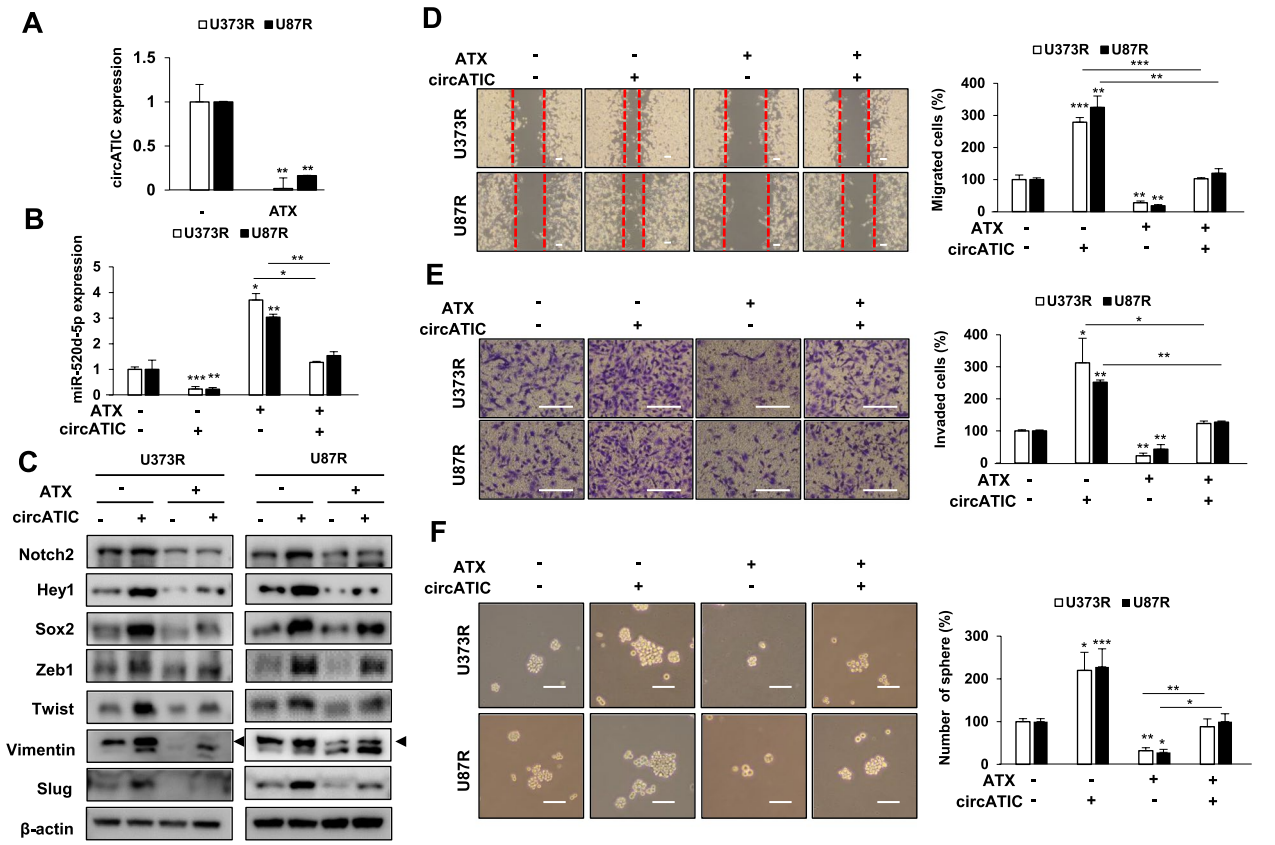

Fig. 7 ATX downregulates tumorigenicity by suppressing the expression of circATIC. **A** After ATX treatment in U373R and U87R cells, the expression of circATIC was confirmed by qRT-PCR. The qRT-PCR results were normalized by GAPDH. **B**-**F** After overexpressing circATIC with or without treatment of ATX, the expression of miR-520d-5p (**B**), stemness and EMT-related factors (**C**), mobility (**D**), invasiveness (**E**), and sphere-forming ability (**F**) were measured by western blot, wound healing (D, Scale bar, 100 μM), matrigel invasion (E, Scale bar, 100 μm), and sphere formation assays (F, Scale bar, 100 μm), respectively. The data are presented as the mean ± SD for triplicate experiments. *$P < 0.05$, **$P < 0.01$, and ***$P < 0.001$. Student's t-test

[35]. The time it takes to complete the entire process is approximately 12 to 15 years or more [35, 36], and the approximate cost of developing a new drug is approximately $2.8 billion [35]. Despite these efforts, the probability of failure in clinical trials is high, so many drug developments are progressing by changing drug use. Drug repurposing involves adapting an already approved drug to treat a new disease or advancing a previously studied but unapproved drug [10]. Between 2007 and 2009, approximately 30–40% of new drugs and biological products approved by the U.S. Food and Drug Administration (FDA) were repurposed drugs, and recently, many drugs are being developed to overcome cancer [11]. For example, a paper by Vineela Parvathaneni et al. describes the effectiveness of amodiaquine (AQ), an FDA-approved anti-malarial drug, in the treatment of breast cancer [37]. In a paper by Yung-Lun Ni et al., it was reported that disulfiram, a drug approved for the treatment of alcoholism, targets cancer stem cells in thyroid carcinoma when combined with copper [38]. A paper by Branco et al. showed that pirfenidone, an FDA-approved drug to treat patients with idiopathic pulmonary, sensitizes NCI-H460 non-small cell lung cancer cells to paclitaxel and the combination of paclitaxel and carboplatin [39].

The standard treatment for GBM, the most malignant tumor, is surgical removal followed by radiotherapy and temozolomide (TMZ) treatment [40]. It is known that some GBMs acquire radiation resistance and have a poor prognosis [7]. Therefore, sensitizers are needed to increase the effectiveness of radiotherapy. We performed a screening using FDA-approved drugs to develop drugs that overcome the radioresistance of GMB (Fig. S2). ATX, which reduced the expression of stemness and EMT-related markers the most (Fig. 1A and S2B), was shown to suppress radioresistant malignancy in vitro and in vivo (Figs. 1 and 2). Clinical relevance was also suggested by showing that ATX effectively suppressed radiation-induced expression of Notch2, Hey1 and sphere-forming ability in 83NS, a patient-derived primary GSC (Fig. 1E, F). In radioresistant GBM cells, TMZ failed to inhibit cell

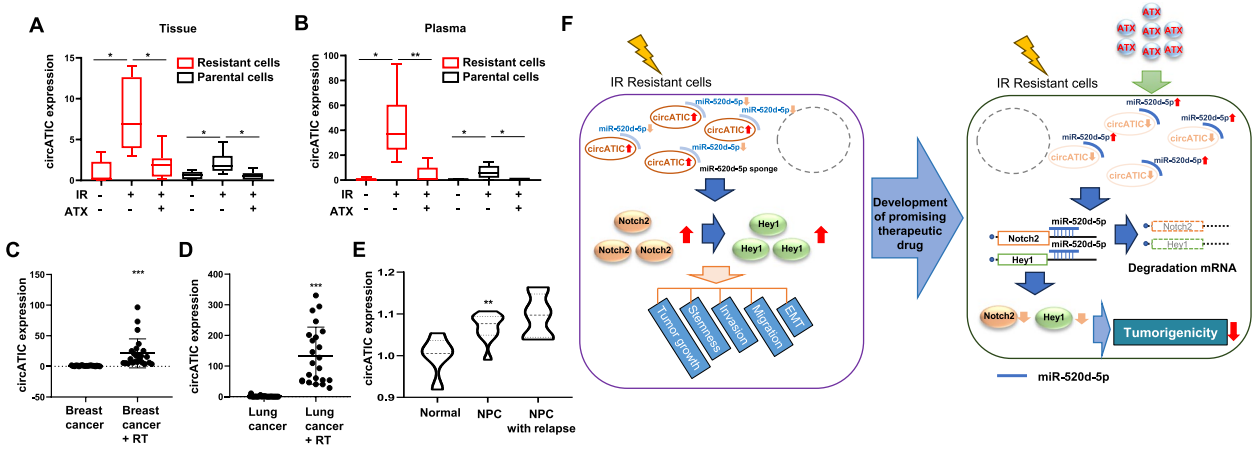

Fig. 8 The clinical applicability of circATIC was verified using experimental animal and patient samples. **A**, **B** The expression of circATIC in tumor tissues (**A**) and plasma (**B**) of ATX-treated xenograft mice was confirmed by qRT-PCR. (circATIC expression in tumor tissues and plasma of indicated groups: resistant cells, $n=5$; resistant cells + IR, $n=5$; resistant cells + IR + ATX, $n=6$; parental cells, $n=5$; parental cells + IR, $n=7$; parental cells + IR + ATX, $n=7$) **C**, **D** The expression of circATIC in the plasma of breast (**C**) and lung cancer (**D**) patients with or without radiotherapy (RT) was confirmed by qRT-PCR. (Breast cancer, $n=20$; Breast cancer + RT, $n=24$; Lung cancer, $n=26$; Lung cancer + RT, $n=24$) qRT-PCR results were normalized by GAPDH. **E** Expression of circATIC was confirmed by GEO database (GSE190271) in nasopharyngeal cancer (NPC). (Normal, $n=5$; NPC, $n=10$; NPC with relapse, $n=8$) The data are presented as the mean ± SD for triplicate experiments. $^{*}P<0.05$, $^{**}P<0.01$, and $^{***}P<0.001$. Student`s t-test. **F** The mechanism of radioresistance in GBM is triggered by circATIC/miR-520d-5p/Notch2-Hey1 axis and ATX is proposed as a drug for drug repurposing

proliferation and tumorigenicity, whereas ATX effectively inhibited radioresistance (Fig. S3). These results showed that ATX has the potential to be an alternative drug to overcome the limitations of TMZ in the treatment of GBM with acquired resistance. In addition, ATX inhibited the target factors Notch2 and Hey1 expressions by inducing miR-520d-5p, ultimately revealing the mechanism of suppressing tumorigenicity in radioresistant GBM cells (Figs. 3, 4 and 5).

circATIC is known as an oncogene in various cancers, including esophageal cancer, bladder cancer, and multiple myeloma [25, 41–44]. In addition, circATIC is known to be associated with resistance such as radioresistance and cisplatin resistance [25, 44]. In our results, the level of circATIC was high in two radioresistant cells and in the mouse tissues injected with radioresistant cells (Figs. 6C and 8A). High expression of circATIC in radioresistant cells decreased the expression of miR-520d-5p, which increased malignancy (Fig. 6). In addition, ATX showed radioresistance suppression efficacy by suppressing the expression of circATIC (Fig. 7). In summary, these results showed that ATX suppresses the expression of circATIC, which acts as a sponge for miR-520d-5p, ultimately suppressing the radioresistance mechanism.

Meanwhile, it is known that it is difficult to properly deliver drugs to the tumor when treating GBM due to the blood–brain barrier (BBB) [45–49]. However, the discovered ATX is a drug that actually passes through the BBB and affects the brain [50–52], so it has great advantages when applied as an anticancer drug. Here, further studies seem necessary to determine how ATX crosses the BBB and affects GBM cells. This study revealed that ATX is involved in radioresistance mechanisms through the circATIC/miR-520d-5p/Notch2-Hey1 signaling pathway (Fig. 8F). Additionally, we demonstrated the applicability of ATX as a sensitizer to assist radiotherapy of GBM, offering potential as a therapeutic target and diagnostic marker for radioresistance.

Conclusion

In summary, our study identified Nothc2, Hey1, and circATIC as key factors for radioresistance, and confirmed that ATX acts as a potent drug to suppress radioresistance. This was analyzed by the mechanism that ATX suppresses radioresistance by inhibiting its direct targets, Nothc2 and Hey1, through the increase in miR-520d-5p expression. Therefore, ATX provides potential as a therapeutic agent for radioresistance and potential as a therapeutic target and diagnostic marker through the circATIC/miR-520d-5p/Notch2-Hey1 signaling pathway of radioresistance.

Abbreviations

ATX	Atomoxetine
CNS	Central nervous system
GBM	Glioblastoma
ADHD	Attention-deficit/hyperactivity disorder
TMZ	Temozolomide
DSBs	Double-strand breaks
RT	Radiotherapy

MTT	3-(4,5-Dimethylthiazol-2-yl)-2,5-diphenyltetrazolium bromide
GSCs	Glioma stem-like cells
hFGF	Human fibroblast growth factor
EGF	Epidermal growth factor
LGG	Low-grade glioma
WT	Wild type
MUT	Mutant type
FDA	Food and Drug Administration
AQ	Amodiaquine
NPC	Nasopharyngeal cancer
BBB	Blood-brain barrier

Supplementary Information

The online version contains supplementary material available at https://doi.org/10.1186/s12964-024-01915-0.

Supplementary Material 1.

Acknowledgements
Not applicable.

Authors' contributions
I.H.B. Supervised the work. I.H.B. and H.J.S. wrote and revised the paper. H.J.S., J.Y.C., and D.H.L. conducted the research and analyzed the data. I.H.B., and H.J.S. designed the experiments and drafted the manuscript. I.H.B., H.J.S., J.Y.C. and D.H.L. designed and performed animal experiments. I.C.S. discussed the results and commented on the manuscript. All authors have read and approved the article.

Funding
This study was conducted with support from the Ministry of Science and ICT (MSIT), the National Research Foundation of Korea, and the Korea Institute of Radiological and Medical Sciences (KIRAMS). [NRF-2021R1A2C2005966(50698–2023), NRF-2017M2A2A7A01018 542(50035–2019), and 50531–2024].

Data availability
No datasets were generated or analysed during the current study.

Declarations

Ethics approval and consent to participate
The clinical data related to this study were approved by the Institutional Review Board (IRB) of the Korea Institute of Radiology and Medical Sciences (KIRAMS) (KIRAMS 2021–04-002–001).

Consent for publication
Not applicable.

Competing interests
The authors declare no competing interests.

Received: 7 August 2024 Accepted: 30 October 2024
Published online: 05 November 2024

References

1. Stupp R, Mason WP, van den Bent MJ, Weller M, Fisher B, Taphoorn MJ, Belanger K, Brandes AA, Marosi C, Bogdahn U, et al. Radiotherapy plus concomitant and adjuvant temozolomide for glioblastoma. N Engl J Med. 2005;352(10):987–96.
2. Davis ME. Glioblastoma: overview of disease and treatment. Clin J Oncol Nurs. 2016;20(5):1–14.
3. Henson JW. Treatment of glioblastoma multiforme: a new standard. Arch Neurol. 2006;63(3):337–41.
4. Miller KD, Ostrom QT, Kruchko C, Patil N, Tihan T, Cioffi G, Fuchs HE, Waite KA, Jemal A, Siegel RL, Barnholtz-Sloan JS. Brain and other central nervous system tumor statistics, 2021. CA Cancer J Clin. 2021;71(5):381–406.
5. Louis DN, Ohgaki H, Wiestler OD, Cavenee WK, Burger PC, Jouvet A, Scheithauer BW, Kleihues P. The 2007 WHO classification of tumours of the central nervous system. Acta Neuropathol. 2007;114(2):97–109.
6. Shimura T, Noma N, Oikawa T, Ochiai Y, Kakuda S, Kuwahara Y, Takai Y, Takahashi A, Fukumoto M. Activation of the AKT/cyclin D1/Cdk4 survival signaling pathway in radioresistant cancer stem cells. Oncogenesis. 2012;1(6):1–9.
7. Ali MY, Oliva CR, Noman ASM, Allen BG, Goswami PC, Zakharia Y, Monga V, Spitz DR, Buatti JM, Griguer CE. Radioresistance in glioblastoma and the development of radiosensitizers. Cancers (Basel). 2020;12(9):1–30.
8. Gu J, Mu N, Jia B, Guo Q, Pan L, Zhu M, Zhang W, Zhang K, Li W, Li M. Targeting radiation-tolerant persister cells as a strategy for inhibiting radioresistance and recurrence in glioblastoma. Neuro Oncol. 2022;24(7):1056–70.
9. Krause M, Dubrovska A, Linge A, Baumann M. Cancer stem cells: radioresistance, prediction of radiotherapy outcome and specific targets for combined treatments. Adv Drug Deliv Rev. 2017;109:63–73.
10. Ajmeera D, Ajumeera R. Drug repurposing: a novel strategy to target cancer stem cells and therapeutic resistance. Genes Dis. 2024;11(1):148–75.
11. Graul AI, Sorbera L, Pina P, Tell M, Cruces E, Rosa E, Stringer M, Castaner R, Revel L. The year's new drugs & biologics - 2009. Drug News Perspect. 2010;23(1):7–36.
12. Jordan VC. Tamoxifen: a most unlikely pioneering medicine. Nat Rev Drug Discov. 2003;2(3):205–13.
13. Sritharan S, Sivalingam N. A comprehensive review on time-tested anticancer drug doxorubicin. Life Sci. 2021;278(119527):1–10.
14. Cortes-Funes H, Coronado C. Role of anthracyclines in the era of targeted therapy. Cardiovasc Toxicol. 2007;7(2):56–60.
15. Aggarwal S, Verma SS, Aggarwal S, Gupta SC. Drug repurposing for breast cancer therapy: old weapon for new battle. Semin Cancer Biol. 2021;68:8–20.
16. Rodriguez S, Hug C, Todorov P, Moret N, Boswell SA, Evans K, Zhou G, Johnson NT, Hyman BT, Sorger PK, et al. Machine learning identifies candidates for drug repurposing in Alzheimer's disease. Nat Commun. 2021;12(1):1–13.
17. Parolo S, Mariotti F, Bora P, Carboni L, Domenici E. Single-cell-led drug repurposing for Alzheimer's disease. Sci Rep. 2023;13(1):1–14.
18. Tomi-Andrino C, Pandele A, Winzer K, King J, Rahman R, Kim DH. Metabolic modeling-based drug repurposing in glioblastoma. Sci Rep. 2022;12(1):1–13.
19. Meissner WG, Remy P, Giordana C, Maltete D, Derkinderen P, Houeto JL, Anheim M, Benatru I, Boraud T, Brefel-Courbon C, et al. Trial of lixisenatide in early Parkinson's disease. N Engl J Med. 2024;390(13):1176–85.
20. Michelson D, Adler L, Spencer T, Reimherr FW, West SA, Allen AJ, Kelsey D, Wernicke J, Dietrich A, Milton D. Atomoxetine in adults with ADHD: two randomized, placebo-controlled studies. Biol Psychiatry. 2003;53(2):112–20.
21. Corona JC, Carreon-Trujillo S, Gonzalez-Perez R, Gomez-Bautista D, Vazquez-Gonzalez D, Salazar-Garcia M. Atomoxetine produces oxidative stress and alters mitochondrial function in human neuron-like cells. Sci Rep. 2019;9(1):1–9.
22. Mao P, Joshi K, Li J, Kim SH, Li P, Santana-Santos L, Luthra S, Chandran UR, Benos PV, Smith L, et al. Mesenchymal glioma stem cells are maintained by activated glycolytic metabolism involving aldehyde dehydrogenase 1A3. Proc Natl Acad Sci U S A. 2013;110(21):8644–9.
23. Kim S, Choi JY, Seok HJ, Park MJ, Chung HY, Bae IH. miR-340-5p suppresses aggressiveness in glioblastoma multiforme by targeting Bcl-w and Sox2. Mol Ther Nucleic Acids. 2019;17:245–55.
24. Yin J, Park G, Kim TH, Hong JH, Kim YJ, Jin X, Kang S, Jung JE, Kim JY, Yun H, et al. Pigment Epithelium-Derived Factor (PEDF) Expression Induced by EGFRvIII promotes self-renewal and tumor progression of glioma stem cells. PLoS Biol. 2015;13(5):1–25.
25. Zhang K, Fan R, Zhao D, Liu P, Yang Z, Liu J, Zhang S, Rao S, Wang Y, Wan L. CircATIC inhibits esophageal carcinoma progression and promotes radiosensitivity by elevating RHCG through sponging miR-10-3p. Thorac Cancer. 2022;13(7):934–46.

26. Seok HJ, Choi JY, Lee DH, Yi JM, Lee HJ, Bae IH. miR-765 as a promising biomarker for low-dose radiation-induced pulmonary fibrosis. Noncoding RNA Res. 2024;9(1):33–43.
27. Bian L, Meng Y, Zhang M, Guo Z, Liu F, Zhang W, Ke X, Su Y, Wang M, Yao Y, et al. ATM expression is elevated in established radiation-resistant breast cancer cells and improves DNA repair efficiency. Int J Biol Sci. 2020;16(7):1096–106.
28. Danielsson F, Peterson MK, Caldeira Araujo H, Lautenschlager F, Gad AKB. Vimentin diversity in health and disease. Cells. 2018;7(10):1–38.
29. Usman S, Waseem NH, Nguyen TKN, Mohsin S, Jamal A, Teh MT, Waseem A. Vimentin Is at the Heart of Epithelial Mesenchymal Transition (EMT) Mediated Metastasis. Cancers (Basel). 2021;13(19):1–26.
30. Zhang N, Hua X, Tu H, Li J, Zhang Z, Max C. Isorhapontigenin (ISO) inhibits EMT through FOXO3A/METTL14/VIMENTIN pathway in bladder cancer cells. Cancer Lett. 2021;520:400–8.
31. Shi Q, Xue C, Zeng Y, Yuan X, Chu Q, Jiang S, Wang J, Zhang Y, Zhu D, Li L. Notch signaling pathway in cancer: from mechanistic insights to targeted therapies. Signal Transduct Target Ther. 2024;9(1):1–37.
32. Bazzoni R, Bentivegna A. Role of notch signaling pathway in glioblastoma pathogenesis. Cancers (Basel). 2019;11(3):1–25.
33. Wu W, Klockow JL, Zhang M, Lafortune F, Chang E, Jin L, Wu Y, Daldrup-Link HE. Glioblastoma multiforme (GBM): An overview of current therapies and mechanisms of resistance. Pharmacol Res. 2021;171:1–26.
34. Chen D, Chou FJ, Chen Y, Huang CP, Tian H, Wang Y, Niu Y, You B, Yeh S, Xing N, Chang C. Targeting the radiation-induced ARv7-mediated circNHS/miR-512-5p/XRCC5 signaling with Quercetin increases prostate cancer radiosensitivity. J Exp Clin Cancer Res. 2022;41(1):1–12.
35. Singh N, Vayer P, Tanwar S, Poyet J-L, Tsaioun K, Villoutreix BO. Drug discovery and development: introduction to the general public and patient groups. Frontiers in Drug Discovery. 2023;3:1–11.
36. DiMasi JA. research and development costs of new drugs. JAMA. 2020;324(5):1–11.
37. Parvathaneni V, Chilamakuri R, Kulkarni NS, Baig NF, Agarwal S, Gupta V. Exploring amodiaquine's repurposing potential in breast cancer treatment-assessment of in-vitro efficacy & mechanism of action. Int J Mol Sci. 2022;23(19):1–21.
38. Ni YL, Chien PJ, Hsieh HC, Shen HT, Lee HT, Chen SM, Chang WW. Disulfiram/copper suppresses cancer stem cell activity in differentiated thyroid cancer cells by inhibiting BMI1 expression. Int J Mol Sci. 2022;23(21):1–14.
39. Branco H, Oliveira J, Antunes C, Santos LL, Vasconcelos MH, Xavier CPR. Pirfenidone sensitizes NCI-H460 non-small cell lung cancer cells to paclitaxel and to a combination of paclitaxel with carboplatin. Int J Mol Sci. 2022;23(7):1–16.
40. Carlsson SK, Brothers SP, Wahlestedt C. Emerging treatment strategies for glioblastoma multiforme. EMBO Mol Med. 2014;6(11):1359–70.
41. Zhou Q, Lei C, Cui F, Chen H, Cao X. Circ-ATIC regulates esophageal squamous cell carcinoma growth and metastasis through miR-1294/PBX3 pathway. Heliyon. 2023;9(1):1–13.
42. Zhang B, Chu W, Li Z, Zhang Y, Zhen Q, Lv B, Liu J, Lu C, Zhao X. Circ-ATIC Serves as a sponge of miR-326 to accelerate esophageal squamous cell carcinoma progression by targeting ID1. Biochem Genet. 2022;60(5):1585–600.
43. Wu B, Wang F, Wang Y, Deng X, Wu W. CircATIC contributes to multiple myeloma progression via miR-324-5p-dependent regulation of HGF. Biochem Genet. 2022;60(6):2515–32.
44. Huang C, Yang Y, Wang X, Chen S, Liu Z, Li Z, Tang X, Zhang Q. PTBP1-mediated biogenesis of circATIC promotes progression and cisplatin resistance of bladder cancer. Int J Biol Sci. 2024;20(9):3570–89.
45. Oberoi RK, Parrish KE, Sio TT, Mittapalli RK, Elmquist WF, Sarkaria JN. Strategies to improve delivery of anticancer drugs across the blood-brain barrier to treat glioblastoma. Neuro Oncol. 2016;18(1):27–36.
46. Sminia P, Westerman BA. Blood-brain barrier crossing and breakthroughs in glioblastoma therapy. Br J Clin Pharmacol. 2016;81(6):1018–20.
47. Schneider SW, Ludwig T, Tatenhorst L, Braune S, Oberleithner H, Senner V, Paulus W. Glioblastoma cells release factors that disrupt blood-brain barrier features. Acta Neuropathol. 2004;107(3):272–6.
48. Da Ros M, De Gregorio V, Iorio AL, Giunti L, Guidi M, de Martino M, Genitori L, Sardi I. Glioblastoma chemoresistance: the double play by microenvironment and blood-brain barrier. Int J Mol Sci. 2018;19(10):1–23.
49. van Tellingen O, Yetkin-Arik B, de Gooijer MC, Wesseling P, Wurdinger T, de Vries HE. Overcoming the blood-brain tumor barrier for effective glioblastoma treatment. Drug Resist Updat. 2015;19:1–12.
50. Gur F, Gur B, Erkayman B, Halici Z, Karakoc A. Investigation of serum and brain superoxide dismutase levels depending on atomoxetine used in attention-deficit/hyperactivity disorder treatment: a combination of in vivo and molecular docking studies. Bioorg Chem. 2020;105:1–7.
51. Fu D, Wu DD, Guo HL, Hu YH, Xia Y, Ji X, Fang WR, Li YM, Xu J, Chen F, Liu QQ. The mechanism, clinical efficacy, safety, and dosage regimen of atomoxetine for ADHD therapy in children: a narrative review. Front Psychiatry. 2021;12:1–7.
52. Bymaster FP, Katner JS, Nelson DL, Hemrick-Luecke SK, Threlkeld PG, Heiligenstein JH, Morin SM, Gehlert DR, Perry KW. Atomoxetine increases extracellular levels of norepinephrine and dopamine in prefrontal cortex of rat: a potential mechanism for efficacy in attention deficit/hyperactivity disorder. Neuropsychopharmacology. 2002;27(5):699–711.

Publisher's Note